ChemPlusChem

Research Article
doi.org/10.1002/cplu.202300711

Chemistry Europe
European Chemical Societies Publishing

www.chempluschem.org

Mixed Matrix Pt-Carbon Nanofiber Polyethersulfone Catalytic Membranes for Glucose Dehydrogenation

Dirk van der Made[+],[a] Ellis van Keulen[+],[a] Tomas van Haasterecht,[a] Johannes Hendrik Bitter,*[a] Martin Weber,[b] and Akbar Asadi Tashvigh*[a]

The advancement of technologies for producing chemicals and materials from non-fossil resources is of critical importance. An illustrative example is the dehydrogenation of glucose, to yield gluconic acid, a specialty chemical. In this study, we propose an innovative production route for gluconic acid while generating H_2 as a co-product. Our concept involves a dual-function membrane, serving both as a catalyst for glucose dehydrogenation into gluconic acid and as a means to efficiently remove the produced H_2 from the reaction mixture. To achieve this two membranes were developed, one catalytically active and one dense aimed at H_2 removal. The catalytic membrane showed significant activity, yielding 16% gluconic acid (t = 120 min) with a catalyst selectivity of 93% and stable performance over five consecutive cycles. Incorporating the H_2 separating membrane showed the significance of H_2 removal in driving the reaction forward. Its inclusion led to a twofold increase in gluconic acid yield, aligning with Le Chatelier's principles. As a future prospect the two layers can be combined into a dual-layer membrane which opens the way for a new production route to simultaneously produce gluconic acid and H_2, using high-throughput reactors such as hollow-fiber systems.

Introduction

The rapid decline in fossil fuels as well as the growing environmental concerns necessitate sustainable alternatives for petrochemical based products.[1,2] Glucose, a readily available natural compound, can be converted into wide spectrum of chemicals.[3] Particularly, the conversion of glucose into gluconic acid, a specialty chemical, is interesting.[4,5] Currently the production of gluconic acid from glucose is performed via aerobic fermentation using microorganisms like *Aspergilus Niger*. Although this process is performed industrially, the production relies on (fed-)batch operation with high aeration cost and heavy downstream processing making the process far from ideal.[6] Another production route is performing the reaction with the aid of an oxidizing agent (e.g., H_2O_2 or O_2) (Scheme 1a). An alternative is the catalytic dehydrogenation of glucose to two valuable products i.e. gluconic acid and hydrogen (Scheme 1b). This reaction can be conducted at milder conditions compared to the use of an oxidizing agent and has a higher atom efficiency.[7–9] However, accumulation of hydrogen can negatively affect the reaction rate and/or shift the thermodynamic equilibrium.[10] In addition, the presence of H_2 can introduce a selectivity challenge with respect to the formation of hydrogenated side products, i.e. sorbitol[11] (Scheme 1c). To overcome these limitations the efficient removal of H_2 is desired. Overall, efficient separation of H_2 during dehydrogenation potentially provides a more sustainable alternative to the current gluconic acid synthesis via fermentation.[12]

The advantages of merging catalytic processes with membrane technology have been well demonstrated.[14,15] The key advantage of catalytic membranes lies in their ability to simultaneously convert reactants and separate (one of the) products in a single step.[16,17] These membranes, typically composed of polymeric materials, are known for their excellent processability, cost-effectiveness, and scalability.[18,19] Incorporation of various fillers (such as catalyst particles) into the polymeric membrane, results in the formation of mixed matrix membranes (MMM).[20] Catalytic membranes represent a common example of MMMs, with the catalyst embedded within the polymer matrix as a filler.[21] Utilizing catalytic membranes helps minimize additional downstream processing steps required for catalyst separation while improving the reaction kinetics. When designing a catalytic MMM, it is essential to consider a few key factors. Firstly, engineering the pore size to facilitate the access of reactants to active sites. Secondly, prioritizing a highly porous structure to maximize the exposure of catalytic sites. Lastly, ensuring a high catalyst loading in the membrane to achieve high activity while maintaining adequate mechanical properties.[22] However, a substantial trade-off emerges between the porosity of the membrane, the loading of the catalyst, and its capability to retain the reactants. This poses a challenge in

[a] D. van der Made,[+] E. van Keulen,[+] T. van Haasterecht, J. H. Bitter, A. A. Tashvigh
Biobased Chemistry and Technology, Wageningen University & Research, Bornse Weilanden 9, 6708 WG Wageningen, the Netherlands
Tel.: (+31)317480694,
Tel.: (+31)317480694,
E-mail: harry.bitter@wur.nl
akbar.asaditashvigh@wur.nl

[b] M. Weber
Performance Materials, BASF SE, G-PM/OU–B001, 67056 Ludwigshafen, Germany

[+] These authors contributed equally to this work.

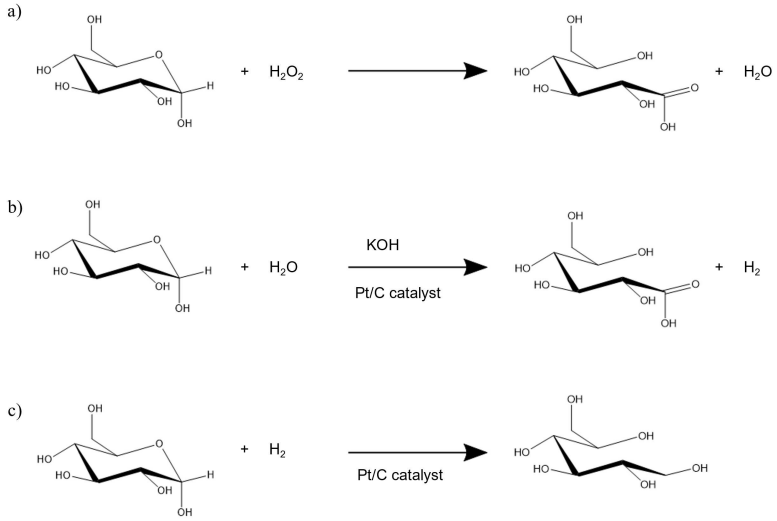

Scheme 1. a) glucose oxidation with H_2O_2, b) glucose dehydrogenation over a Pt/Carbon catalyst under alkaline conditions and c) glucose hydrogenation over Pt/Carbon catalyst in the presence of H_2.[13]

designing an efficient catalytic membrane system. Hence, a potential solution could involve the design of a dual layer membrane, where the upper layer consists of high porosity and catalyst loading while the denser layer underneath remains only permeable to (one of) the products, namely hydrogen in this case (Figure 1).

Platinum (Pt) is typically a good catalyst for oxidation reactions, expressing high activity and stability.[23] Specifically, for the dehydrogenation of glucose, platinum demonstrates excellent activity and selectivity towards gluconic acid.[24] Polyethersulfone (PESU) stands out as an excellent polymer for MMM due to its high mechanical and pH stability, which are often critical for catalytic processes.[25,26] Therefore, the combination of Pt and PESU could serve as a platform for the dehydrogenation of glucose.

In this study, we report the preparation of a simplified dual layer membrane system for catalytic dehydrogenation of glucose. Here, we initially incorporated Pt particles onto a carbon nanofiber (CNF) support for two primary purposes: to increase Pt loading in the MMM and to improve the accessibility of Pt particles during the reaction. CNFs are known for their high surface area, thermal stability, chemical inertness, and porosity.[27] The Pt-CNF were then incorporated in PESU to form the catalytic membrane for glucose dehydrogenation. The second membrane was made from PESU to solely permeate the H_2 while retaining the reaction content. These membranes were characterized using multiple analytical methods, such as x-ray diffraction, chemisorption and physisorption to explain the performance of the membranes. Moreover, the configuration of the two membranes and its influence on the reaction

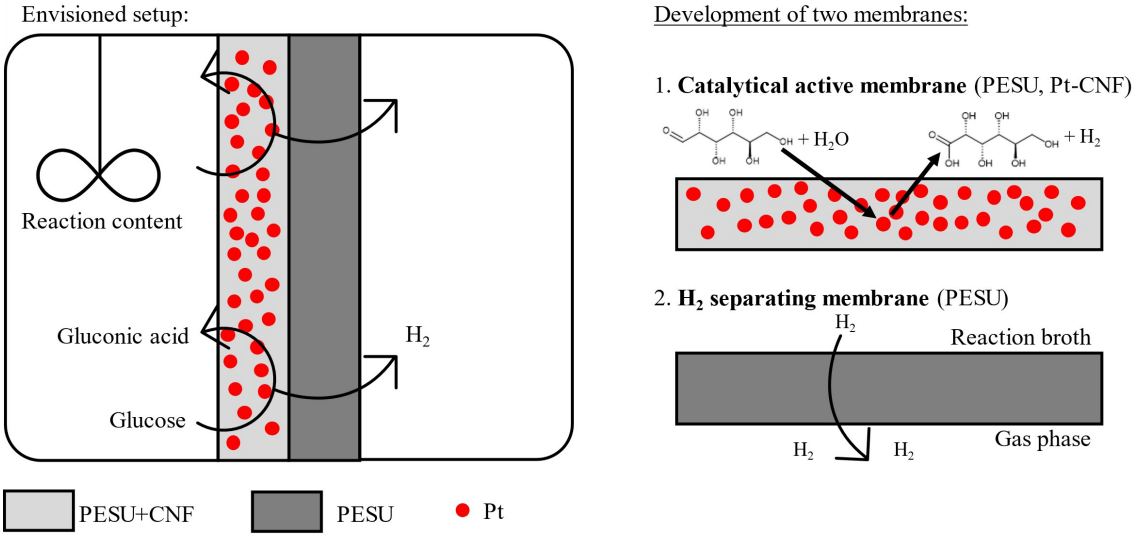

Figure 1. Schematic of the envisioned dual layer membrane system for catalytic dehydrogenation of glucose including a description of the two different membranes developed.

conversion was investigated. Finally, to determine the effectiveness of the membranes, the reaction kinetics and stability of the catalytic membranes were also studied.

Experimental Section

Materials

Polyethersulfone (Ultrason® E 6020 P, BASF) was used as polymer matrix. Dimethylformamide (DMF, ≥99.8%, Sigma-Aldrich) and tetrahydrofuran (THF, ≥99.9%, Sigma-Aldrich) were used as solvents for membrane fabrication. CNF-HCl (<90 μm) were used as catalyst support while tetraamine platinum (II)nitrate (≥99.995% trace metal basis, Sigma-Aldrich) was utilized as platinum precursor. KOH (≥85%, Sigma-Aldrich) was utilized as a base for adjusting the pH of the reaction. D-gluconic acid sodium salt (≥99%, Sigma-Aldrich) was used for HPLC calibration standard while sulfuric acid (≥98%, Supelco) was used for the HPLC mobile phase. Carbon nanofibers (CNF) were prepared in-house by chemical vapour deposition from a mixture of hydrogen (102 mL/min), nitrogen (450 mL/min), and carbon monoxide (260 mL/min) at 550 °C at 3 bar for 24 h over a reduced 5 wt% Ni/SiO2 catalyst (3 g). Afterwards, to remove SiO_2 and Ni the as prepared CNF was first refluxed three times in 1 M KOH for 1 h followed by refluxing in 37% HCl solution for 1.5 h. D-glucose (≥99.5%, Sigma-Aldrich) was used as the main reactant.

Catalyst Synthesis

The catalyst was synthesized through incipient wetness impregnation (IWI). Firstly, 0.95 g of CNF was weighed in a round bottom flask. Next, 0.0992 g of tetraamine platinum (II)nitrate precursor was dissolved in 0.7 mL of DI water. The precursor solution was slowly added to the CNF and occasionally shaken vigorously to distribute the solution evenly. The CNF was then dried overnight at 110 °C to evaporate all the water. The dry CNF was placed in a pre-dried plug flow reactor, which was flushed with N_2 to remove any oxygen. The CNF was reduced in this reactor at 100 mL/min of 30% H_2 for 1 h at 200 °C with a heating ramp of 10 °C/min.

Membrane Preparation

Two types of membranes were designed. One H_2 separating (dense) membrane to continuously remove the produced H_2, while retaining the reaction solution and a catalytic MMM intended for catalyzing the dehydrogenation reaction. For the H_2 separating membranes, 18 wt% PESU was dissolved in solvent mixture of DMF: THF (90:10, wt%). After achieving a homogenous solution, it was degassed overnight. Next, the solution was manually casted with a film casting knife (BYK) on a glass plate with a thickness of 300 μm. The film was left for 1 minute for THF evaporation and subsequently immersed in a water bath for 10 minutes to induce phase inversion. The membrane was kept overnight in a separate DI water bath to fully remove the residual solvent. Finally, the membranes were cut into circles with diameter of 45 mm and air dried.

For the preparation of MMMs, the optimization of CNF loading was the initial step. Various amounts of CNF and PESU were separately dissolved in DMF (as outlined in Table 1) and mixed together. The resulting solution was sonicated for 5 minutes and directly casted onto a glass plate with a thickness of 400 μm. The membranes were immediately immersed in a water bath for 10 minutes and left overnight in a separate DI water bath. The membrane with a 50% CNF loading (CNF50) was subsequently employed for the preparation of catalytic membranes, as higher CNF loadings were found to compromise the mechanical stability of the membranes.

Table 1. Composition of the casting solutions.

Membrane	PESU content (g)	CNF content (g)	DMF content (g)
H_2 separating membrane	18	0	73.8 (+8.2 THF)
CNF0	10	0	90.0
CNF1	10	0.1	90.0
CNF5	10	0.5	90.0
CNF10	10	1.1	90.0
CNF20	10	2.4	90.0
CNF50	10	10	90.0
CNF75	10	30	90.0

Catalytic Glucose Dehydrogenation

All reactions were conducted at room temperature, using a 3.3 g/L active catalyst concentration based on the active surface area (H_2 chemisorption) in a reaction mixture consisting of 0.33 M KOH and 0.06 M glucose. Each experiment was done in triplicate.

Kinetic study: In each experiment, 0.5 mL of the reaction mixture were introduced into individual 1.5 mL vials and subjected to argon purging. Afterward, the catalyst (Pt-CNF) was introduced, and the vials were placed on a rolling stirrer. The reactions were conducted separately for intervals of 5, 10, 15, 30, 60, 90, and 120 minutes.

Headspace test: In 1.6 mL vials, either 0.5, 1.0, or 1.5 mL of the reaction mixture was added and subsequently purged with argon. The catalyst (Pt-CNF) was introduced, and the vials were placed on a rolling stirrer. Reactions were performed for 2 h.

Incorporation of H_2 separation membrane: A H_2 separating membrane was placed into an Amicon Stirred Cell Model 8010 in the gas phase, and 12 mL of the reaction mixture was introduced. The liquid to gas volume ratio was 15:1. Subsequently, catalyst particles (Pt-CNF) were added, and the mixture was stirred for 2 h under 1 bar of Argon (visualised in Figure 2).

Catalytic membranes and stability measurements: In a 20 mL tube, 5 mL of the reaction mixture was dispensed and then purged with argon. Subsequently, 81.3 mg of catalytic membrane (equivalent to approximately 3.3 g/L based on the active catalytic surface determined with H_2 chemisorption) was added to the solution. The mixture was stirred for either 2 or 4 h.

For the stability test, the same conditions were applied, but the experiment was repeated five times using the same catalytic membrane, with each run lasting for 2 h.

Characterization

X-ray diffraction (XRD) was performed on a Bruker D8 Advance to determine the crystalline phases in both the catalyst and the membranes. CNF and Pt particles were identified.[28,29] The average platinum crystallite size was calculated using the Scherrer equation.

$$\tau = \frac{K\lambda}{\beta cos\theta} \quad (1)$$

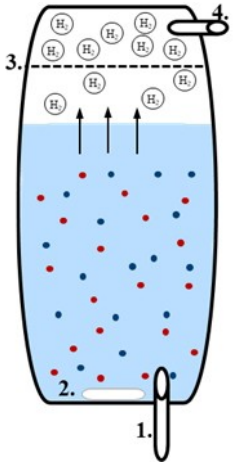

Figure 2. Schematic of Amicon reactor with the H_2 separating membrane in the gas-phase, wherein: 1 = argon inlet, 2 = stirring rod/bar, 3 = H_2 separation membrane and 4 = outlet.

Where τ is the mean crystallite size, K denotes the shape factor, λ is the x-ray wavelength, β represents the peak width at half-height and θ is the Bragg angle.

N_2-physisorption analysis was performed utilizing a Micromeritics Tristar II Plus instrument to determine the BET surface area for both the catalyst and the membranes. To prepare the samples for analysis, they were dried and degassed overnight at 180 °C under vacuum conditions before measurements were taken.

Transmission electron microscopy (TEM) was employed to examine the structural characteristics of the catalyst and quantify the size of platinum particles. Imaging was conducted utilizing a JEOL JEM-1011 instrument. Particle size analysis was conducted by measuring 254 individual particles using ImageJ software.[30] Sample preparation involved dispersing the catalyst (Pt-CNF) in ethanol through ultrasonic treatment, followed by the deposition of 6 μL of the prepared sample onto a Formvar carbon-coated copper grid. Subsequently, the grid was allowed to air dry at room temperature.

Field emission scanning electron microscopy (FESEM, FEI Magellan 400 FESEM) measurements were conducted to examine the morphology of the membranes. For preparation, the membrane samples were freeze dried and fractured in liquid nitrogen.

The active (metal) surface area of both the catalyst and catalytic membrane was determined using H_2 chemisorption. Prior to analysis, the samples underwent a sequence of steps for preparation. They were initially flushed with helium at 100 °C, followed by two cycles of evacuation under vacuum at the same temperature. Subsequently, the samples were subjected to calcination in H_2 at 150 °C for 120 minutes to eliminate any platinum oxide. Afterward, evacuations were performed again, first at 350 °C for 120 minutes and then at 35 °C for 30 minutes to remove any remaining H_2. A leak test was conducted to initiate the measurement process. The initial isotherm provided data on total gas uptake, followed by another evacuation, and the subsequent measurement of the second isotherm. Finally, particle sizes and dispersion were calculated based on known platinum loading and sample weight.

The thermal stability of the membranes were assessed by thermogravimetric analysis (TGA) using a Mettler Toledo TGA/DSC. A crucible containing membrane samples was subjected to a N_2 flow. The temperature program involved an initial 5 K min^{-1} ramp to 373 K, followed by an isothermal period lasting 30 minutes. The sample was then cooled down to 303 K at a rate of 10 K min^{-1}. This was followed by a 5 K min^{-1} ramp to 1173 K, and a final isothermal period of 5 minutes.

The reaction yield, selectivity and degradation products were analyzed on a Dionex UltiMate 3000RS high-performance liquid chromatography (HPLC) system. Samples containing CNF–Pt particles were filtered using a 0.2 μm filter before injection. The HPLC was run at 0.5 mL/min of 0.55 mM H_2SO_4, for 30 minutes at 35 °C with an injection volume of 10 μl using an Aminex HPX-87H 300×7.8 mm column. The concentrations of glucose and fructose were measured by refractive index (RI) detector, while the concentrations of gluconic acid and degradation products were determined by an ultraviolet (UV) detector at 210 nm.

Results and Discussion

Catalyst Synthesis

Figure 3 displays the XRD patterns of both pristine and platinum loaded CNF through IWI. The pristine CNF shows peaks at $2\theta = 26°$ and $2\theta = 43°$ corresponding to the (002) and (101) reflections of graphite, respectively. The same peaks are present for the Pt-CNF catalyst, with several additional peaks (green dots in Figure 3) which can be attributed to Pt. Most of the additional peaks were found to be related to metallic Pt with a small amount of Pt-oxide ($2\theta = 28°$), indicating successful incorporation of platinum particles onto the CNF support. Based on the peak broadening of the Pt reflection the average crystallite size was estimated to be 9 nm.

The structure and particle size of CNF-pt particles were examined by transmission electron microscope (TEM) as depicted in Figure 4(a,b and c). The typical CNF structure, featuring stacked graphene plates and a tunnel-like void at the core can be seen in Figure 4a. The deposition of platinum onto the CNF is evident, as indicated by the dense, dark dots observed in Figure 4b. The average Pt particle size based on TEM for is 6.8 nm, 7.1 nm and 7.4 nm based on number average, surface average and volume average, which is in good agreement with XRD.

Chemisorption was performed on the catalyst (Pt-CNF particles) to examine the active surface area and the dispersion of the platinum. The results from the measurement yielded a surface average particle size of 12 nm corresponding to a Pt dispersion of approximately 9 %. Dispersion is a measure for the fraction of surface atoms compared to the total atoms surface and bulk. It can be determined from the amount of chemisorbed H_2 (derived from the intercept of the H_2 adsorption isotherm (Figure 4d)), the stoichiometry factor and the amount of Pt present in the sample. The low Pt dispersion is the result of relatively large nanoparticle size, which are generally more stable. Low dispersions of Pt can be resolved by pretreatments of the CNF by acid (increasing the hydrophilicity of the fibers), the latter is out of the scope of this study.

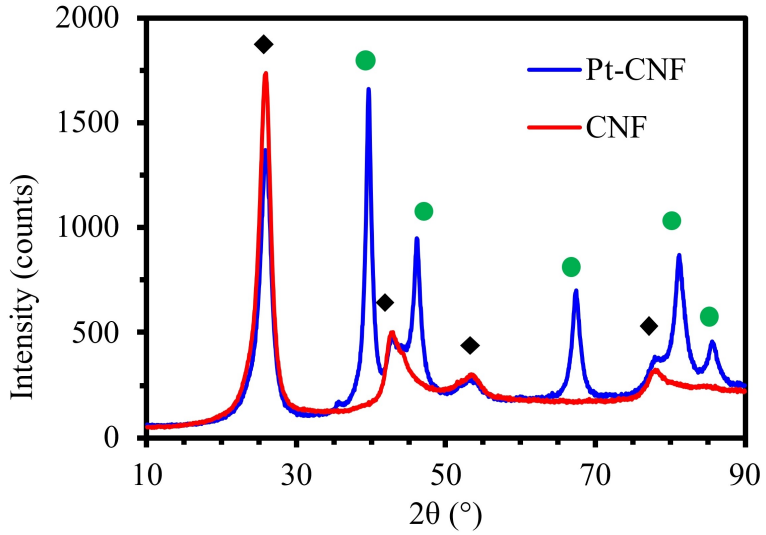

Figure 3. XRD diffractogram of unmodified and platinum loaded CNF (with indicating carbon ♦[29] and metallic Pt • phases[28]

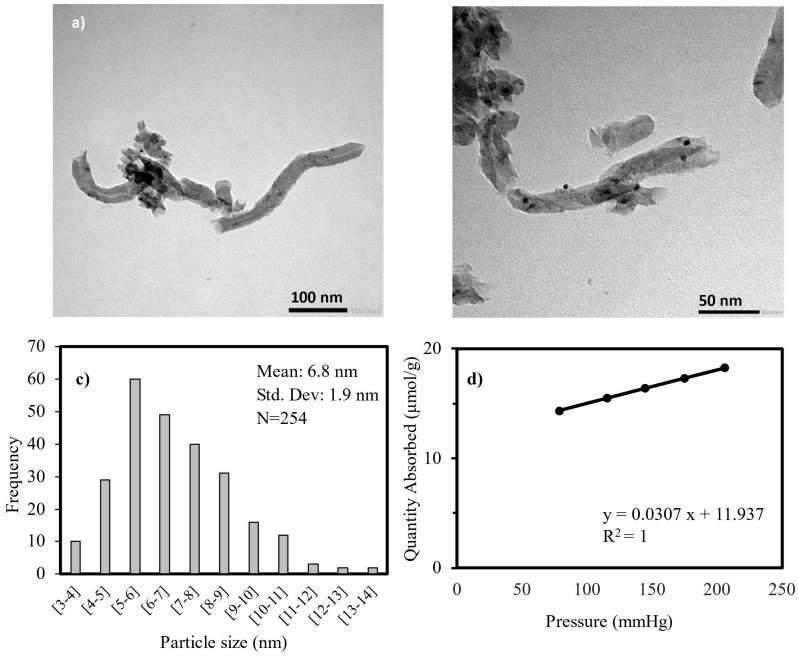

Figure 4. The TEM images of a) pristine CNF and) Pt-CNF catalyst and c) particle size distribution of Pt particles (N = 254) and the d) H_2 chemisorption analysis for Pt-CNF.

Membrane Characterization

The initial focus of the membrane synthesis was on the production of a MMM with the necessary properties for subsequent testing. I.e. achieving a highly porous structure and maximizing the exposure of catalytic sites which necessitates a low polymer concentration and high CNF loading. Multiple MMMs were prepared using 10 wt% polymer concentration, allowing for the incorporation of up to 75 wt% CNF within the membranes. These MMMs, as illustrated in Figure 5, were then employed for further analysis and testing.

MMMs were made at multiple CNF loadings and their textural properties were analyzed using N2-physisorption. Figure 6 shows the BET surface area of pure CNF and various MMMs. Given the high surface area of CNF, the surface area of the membranes increases along with the CNF concentration. From the highest concentration membranes (CNF50 and CNF75) it becomes clear that not all of the CNF surface is available in the MMMs when comparing to pure CNF. This could be attributed to partial coverage and/or pore blocking of the CNF at higher concentrations. Although some of the CNF surface is lost, for both the CNF50 and CNF75 membranes approximately 45% of the surface is still accessible and

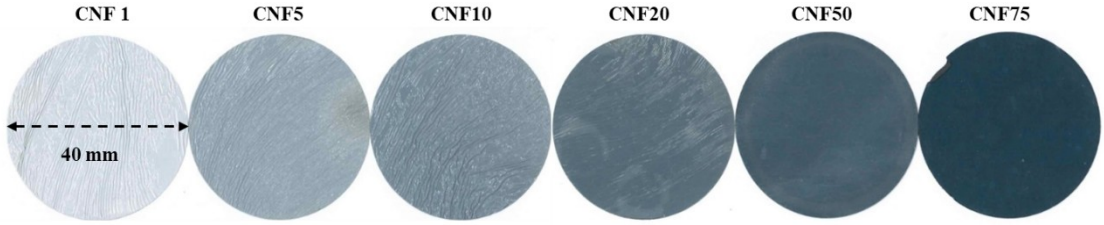

Figure 5. Appearance of the MMMs composed of PESU and different concentrations of CNF.

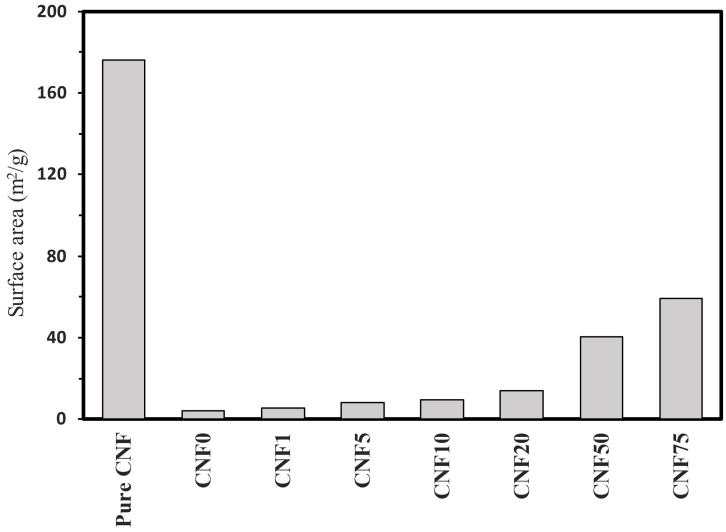

Figure 6. BET surface measured using N_2 physisorption of pure CNF and MMMs with different CNF concentrations.

available for reactants (i.e., CNF75 exhibits 59 m^2/g vs 132 m^2/g theoretical value and CNF50 shows a surface area of 40 m^2/g vs 88 m^2/g theoretical value).

The average pore size of the CNF50 and CNF75 membranes was found to be 13 nm . With a size of roughly ~1 nm, the main reactant glucose can diffuse through the membrane matrix towards active sites. Lastly, given the poor physical/mechanical properties of the CNF75 membrane, the handling of CNF75 was difficult and 50% CNF loading was determined as the optimal CNF concentration.

Figure 7 shows SEM image of the surface and cross section of CNF0 and the catalytic (CNF50-Pt) membranes. Both membranes seem to have similar front and back side morphologies. However, CNF0 shows a consistent cross section structure with abundant finger like macrovoids across the membrane thickness measuring at approximately 40 μm. Conversely, CNF50-Pt exhibits a disordered structure featuring finger like macrovoids at the upper surface and large and disordered macrovoids underneath. Moreover, as expected, the thickness of CNF50-Pt is much higher than the CNF0 at 105 μm

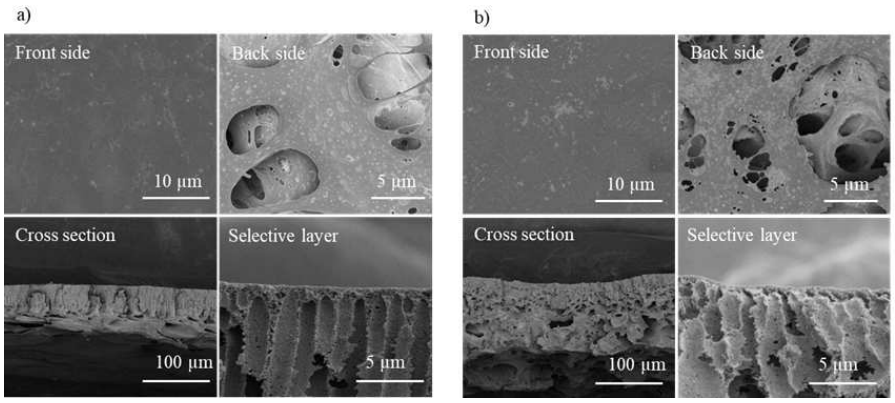

Figure 7. Morphology of a) CNF0 and b) CNF50-Pt.

due to the presence of CNF, which makes the membranes less dense.

The incorporation of active platinum species in the MMMs was examined using XRD, as presented in Figure 8. In the XRD pattern of PESU (CNF0) no crystalline structure can be seen. In contrast to CNF0, CNF50 exhibits a distinct peak at $2\theta = 26°$, attributable to the (002) reflection of CNF. Upon comparing CNF50 and CNF50-Pt, the presence of metallic platinum peaks becomes evident, confirming the incorporation of platinum within CNF50-Pt while preserving the catalytically active platinum components.

Chemisorption was used to further examine if the incorporation of the catalyst into the MMM was successful. The average platinum particle size and dispersion were found to be 12 nm and 10%, which closely aligns with the values obtained for the Pt-CNF particle (12 nm, 9%). This observations suggest that the active surface and structural characteristics of the catalyst remained largely unaltered during its incorporation into the MMM. Consequently, it can be inferred that Pt-CNF can be effectively integrated into PESU to form a catalytic MMM, without significantly altering the properties of the catalysts active surface.

Figure 9 shows the mass reduction of both CNF0 and CNF50 as a function of temperature through thermogravimetric analysis (TGA). Neither samples show significant mass loss until 400 °C. At higher temperatures both samples decompose although at different rates. As expected CNF50 experiences less weight loss than CNF0 due to the presence of CNF.

Catalytic Dehydrogenation of Glucose

Before conducting any reactions involving the catalytic membrane, an initial investigation of the dehydrogenation reaction was conducted using a pristine Pt-CNF catalyst. This section discusses the analysis of reaction kinetics, selectivity, and the

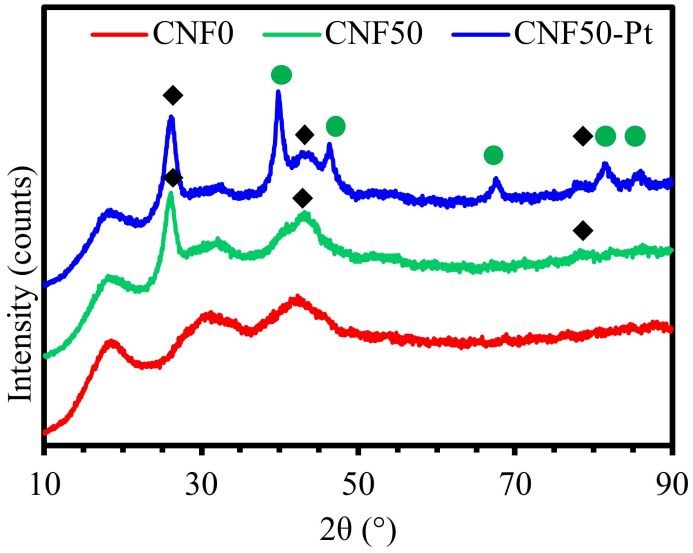

Figure 8. XRD diffractograms of CNf0, CNF50 and CNF50-Pt membranes (with indicating carbon ♦[29] and metallic Pt •[28]).

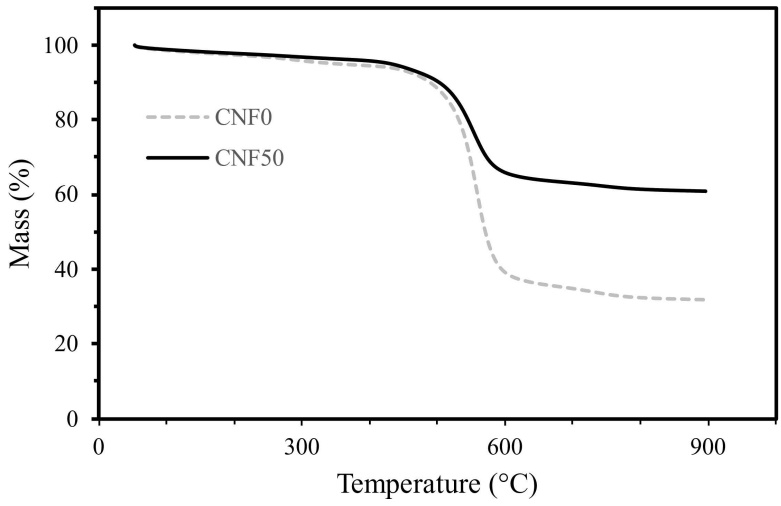

Figure 9. Thermogravimetric analysis (TGA) of CNF0 and CNF50 membranes performed in duplo.

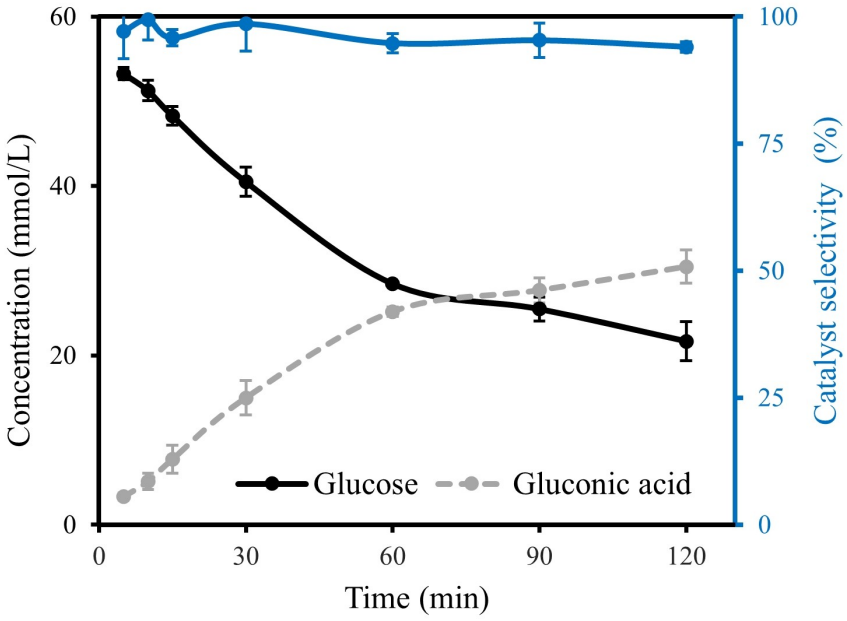

Figure 10. Glucose and gluconic acid concentration (mmol/L) and catalyst selectivity (%) towards gluconic acid (mean ± SD) over time during the dehydrogenation (conditions: 0.33 M KOH, 0.06 M glucose, RT, 3.3 g/L pure Pt-CNF catalyst) performed in triplo.

influence of H_2 gas evolution, as well as its permeation through the H_2 separating membrane and its effect on the reaction conversion.

Reaction Kinetics

Batch reactor experiments were conducted to study gluconic acid production over time. As shown in Figure 10 glucose is consumed, while gluconic acid is produced. The initial reaction rate is stable for the first 60 minutes of the reaction at a rate of 0.40 mM/min ($R^2 = 0.99$ fit). Later the reaction is inhibited, which could be caused by multiple mechanisms such as: the consumption of reactant (glucose), product inhibition, over-pressure through H_2 formation and/or depletion of the base. For the latter Abbadi & van Bekkum[31] who performed the reaction by supplying molecular oxygen illustrated that without pH control, inhibition of the catalyst was observed below a pH of 7. Here it is hypothesized that under acidic conditions the produced gluconic acid is inhibiting the catalyst. The glucose conversion is directly related to the formation of gluconic acid, illustrated by a high catalyst selectivity over time. The catalyst selectivity is corrected for the formation of fructose as fructose is formed due to the enolization of glucose under alkaline conditions,[32] and the formation is independent of the catalyst. From Figure 10 it becomes clear that the catalyst selectivity towards gluconic acid remains high and relatively stable over the whole reaction time.

Complementary is Table 2, where the molar concentrations are shown of the main components in the reaction mixture at t = 120 min. Illustrating that no significant degradation or side-products are formed, besides fructose (via enolization). However, no sorbitol formation was observed, which could be due to low reaction temperatures and/or relatively low partial hydrogen pressures. After two hours the catalyst selectivity of the Pt-CNF catalyst towards gluconic acid was 94% with a gluconic acid yield of 51%.

Table 2. Molar concentrations (mean ± SD) of glucose and its conversion/degradation products at t = 120 min performed in triplo (conditions: 0.33 M KOH, 0.06 M glucose, RT, 3.3 g/L pure Pt-CNF catalyst).

Compound	Concentration (mmol/L)	± SD
Glucose	21.7	2.3
Gluconic acid	30.5	2.0
Fructose	5.92	0.15
Glucuronic acid	0.84	0.07
Glucaric acid	1.04	0.12
Glycolic acid	0.41	0.02
Formic acid	0.91	0.02
Catalyst selectivity (%)	94	

Comparison of catalyst performance is complicated due to the effects of different metal precursors, support properties, dispersion and differences in reaction conditions (e.g., supply of molecular oxygen or pH). A selection of performances of catalysts on carbon supports for the conversion of glucose into gluconic acid is shown in Table 3. Comparing shows that our Pt-CNF catalyst has a relatively low conversion at t = 120 min (54%), but exhibits a high selectivity towards gluconic acid.

Table 3. Comparison of catalyst performance for the conversion of glucose into gluconic acid.

Catalyst	P (O_2) (bar)	Temp (K)	Glucose (t = 0) (mol/L)	Time (h)	pH	Conversion (%)	Selectivity (%)	
5% Pt/C	1	333	0.6	7	9	85	77	[33]
5% Pt/C	–	298	0.07	1	13.5	97	87	[13]
Pd/Cellulose	–	298	0.1	3	< 9	100	91	[34]
Pt-CNF	–	293	0.06	1	13.5	54	94	This work

* Excluding fructose formation.

Effects of H_2 on Conversion

The impact of H_2 formation on reaction conversion was studied by varying the ratio of gas headspace in the batch reactor to the volume of the liquid reaction mixture and therefore altering the hydrogen partial pressure. As depicted in Figure 11, as the liquid/gas volume ratio increases, there is less available space for H_2 gas, resulting in higher H_2 partial pressure. The calculated (with the ideal gas law) partial pressure of hydrogen of the 15:1 (liquid:gas) volume ratio vial is almost 7 times higher compared to the 0.5:1 vial (liquid:gas). While the gluconic acid yield for the volume ratio of the 0.5:1 vial (liquid:gas) is 5 times higher compared to the 15:1 vial (liquid:gas). Illustrating that a high partial pressure inhibits the reaction rate, preventing further conversion towards gluconic acid. This results demonstrate a direct correlation between reaction conversion and headspace volume. Hence, it is important to constantly remove the produced H_2 gas during the reaction in order to achieve higher gluconic acid yields while making use of the total reactor volume.

H_2 Separation Using H_2 Separating Membrane

The efficiency of the H_2 separating membrane in removing the produced H_2 gas during the glucose dehydrogenation reaction was evaluated in a membrane reactor vessel. Two different setups were compared, namely one closed vessel (without the H_2 separating membrane) and one open vessel under 1 bar of argon with the membrane in the gas phase as illustrated in Figure 2. It should be noted that the addition of 1 bar of inert gas (argon), has a negligible effect on the state of equilibrium in the reaction[35] and therefore, only the effects of membrane is being studied here. Both with the same liquid-to-gas volume ratio of 15:1. As shown in Figure 12, the open vessel with the membrane in the headspace has almost a factor of 2 higher gluconic acid yield compared to the closed vessel. Confirming that H_2 gas can successfully permeate through the membrane and that the removal of H_2 increases the reaction rate. The latter follows the principles of Le Chatelier, which states that increasing pressure will shift the equilibrium towards the side of fever molecules. The removal of hydrogen disturbs the dynamic equilibrium, which thereby drives the equilibrium towards the

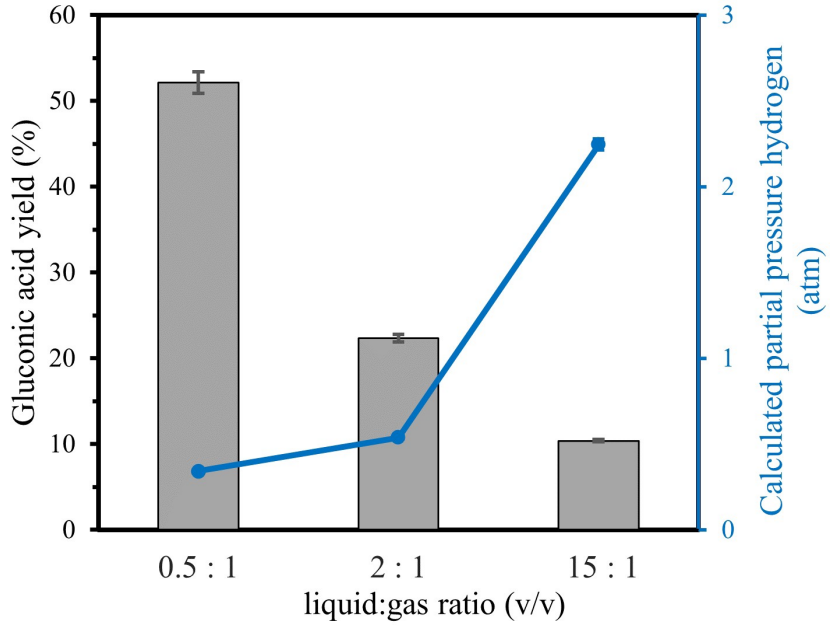

Figure 11. The gluconic acid yield (mean ± SD) and calculated partial pressure for hydrogen (atm) for the dehydrogenation of glucose at different liquid:gas volume ratios (conditions: 0.33 M KOH, 0.06 M glucose, RT, 3.3 g/L pure Pt-CNF catalyst) performed in triplo.

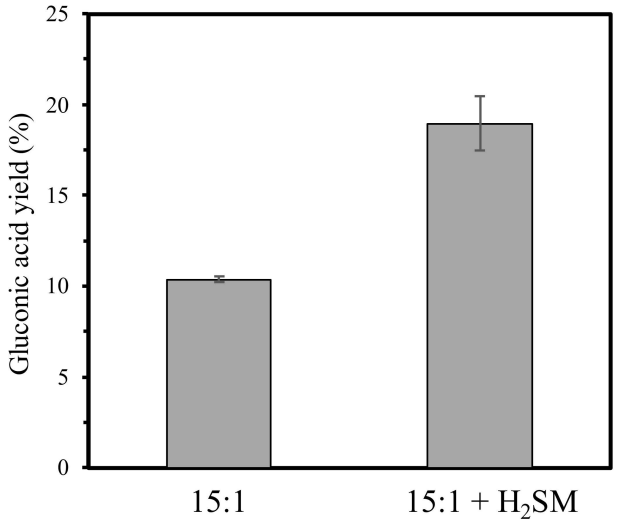

Figure 12. The gluconic acid yield (mean ± SD) for the dehydrogenation of glucose at a 15:1 liquid/gas volume ratio with a closed vessel (15:1) or with the H_2 separating membrane (H_2SM) in the headspace (15:1 + H_2SM) (conditions: 0.33 M KOH, 0.06 M glucose, RT, 3.3 g/L pure Pt-CNF catalyst, 1 bar argon in case of dense membrane) performed in triplo.

right side (of gluconic acid). The increase of the gluconic acid yield in Figure 12 illustrates the importance of removing hydrogen from the reactor for dehydrogenation reactions.

Catalytic Membrane Testing

Activity and selectivity

In contrast to previous experiments where Pt-CNF particles were used as catalyst, here catalytic membranes were added to the reaction mixture to facilitate the reaction. Figure 13 shows the gluconic acid yield achieved by the catalytic membrane (CNF50-Pt). The observed gluconic acid yield is 16% and 27% after 120 min and 240 min, respectively. By analysing the molar concentrations at t = 120 min, it becomes clear that the reaction exhibits a high selectivity towards gluconic acid (Table 4). The selectivity at t = 120 min is similar to the pure Pt-CNF catalyst (Table 2). Again no sorbitol formation was observed. The selectivity at t = 240 min decreases as more degradation products, such as formic acid are observed.

Comparing the gluconic acid yield at t = 120 min in this experiment to the pure Pt-CNF catalyst depicted in Figure 10, the yield of the pure Pt-CNF is 3 times higher compared to the catalytic membrane. Both reactions are performed under the same liquid/gas ratios and the amount of active catalyst added to the reactions are the same. In addition, this reduced conversion may not be attributed to changes in the catalyst structure during MMM synthesis, as the catalyst properties remained unchanged according to the chemisorption data. It is more likely that the complex structure of porosity and voids within the catalytic membrane, in contrast to the pure CNF, leads to diffusion limitations in the reaction using catalytic membranes. Mass-transfer limitations could potentially be resolved by the design of a catalytic hollow-fiber membrane and the associated increase in convection.

Stability

The stability of the catalytic membrane was assessed by tracking its performance through multiple cycles. The results presented in Figure 14 show that there was no significant degradation observed in the catalytic activity of the membrane. The conversion towards gluconic acid remains relatively con-

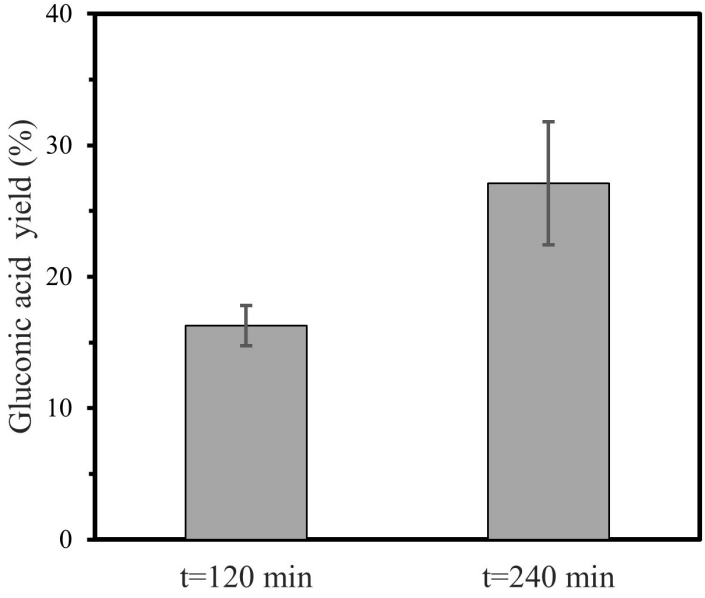

Figure 13. The gluconic acid yield (mean ± SD) using the catalytic membrane, membrane loading adjusted accordingly to the catalytically active surface area (H_2 chemisorption) to correspond to 3.3 g/L of pure Pt-CNF (conditions: 0.33 M KOH, 0.06 M glucose, RT) performed in triplo.

Table 4. Molar concentrations (mean ± SD) of glucose and its conversion / degradation products using the catalytic membrane at t = 120 min and t = 240 min (conditions: 0.33 M KOH, 0.06 M glucose, RT, membrane loading adjusted accordingly to the catalytically active surface area (H_2 chemisorption) to correspond to 3.3 g/L of pure Pt-CNF) performed in triplo.

Compound	t = 120 (min)		t = 240 (min)	
	Concentration (mmol/L)	± SD	Concentration (mmol/L)	± SD
Gluconic acid	9.75	0.82	16.3	2.5
Glucose	42.3	1.1	31.7	2.6
Fructose	7.20	0.34	9.70	0.10
Glucuronic acid	0.61	0.11	1.31	0.07
Glucaric acid	0.49	0.07	0.94	0.16
Glycolic acid	0.64	0.08	1.40	0.12
Formic acid	1.22	0.30	2.52	0.33
Catalyst selectivity (%)	93		88	

sistent across the 5 consecutive runs. The main factor contributing to the stability could be the relatively large particle size of the platinum. Furthermore, embedding of the catalyst in the membrane structure could attribute to the stability of the catalytic membrane. Finally, the stationary nature of the catalytic membrane prevents mechanical degradation, which is often observed in slurry reactor systems.

Conclusions

In this study, novel catalytic MMMs and H_2 separating membranes resembling dual-layer membranes were synthesized for simultaneous conversion and separation of H_2 in the dehydrogenation of glucose. Using the knife casting method, MMMs with up to 50% of CNF and sufficient mechanical properties were obtained. Incorporation of active Pt species in the polymeric matrix of the MMM was found to be successful according to XRD and chemisorption. The catalytic membrane was found to selectively produce gluconic acid (93%) under relatively mild conditions. Although the gluconic acid yield of the catalytic membrane was found to be 3 times lower than the pure Pt-CNF catalyst, the high selectivity and stability give this material opportunities for further use. Hydrogen buildup within the reactor needs to be prevented as it severely hinders the reaction. A H_2 separating membrane was developed to remove the hydrogen from the reactor mixture, which increased the gluconic acid yield by a factor of 2. Combining the two membranes as a dual-layer membrane enables future applications in hollow fiber reactor setups, which could potentially by further optimization solve the diffusion limitations within the membrane.

Conflict of Interests

The authors declare no conflict of interest.

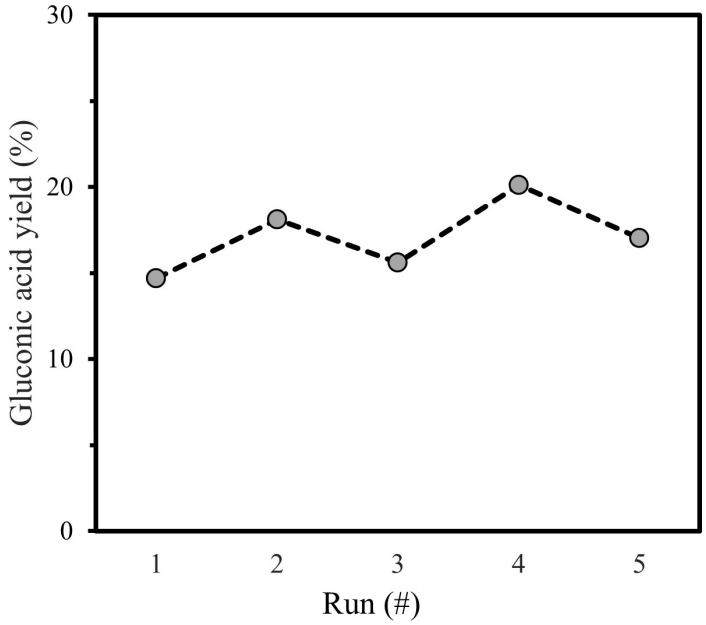

Figure 14. Gluconic acid yield (%) using the same catalytic membrane over 5 runs, membrane loading adjusted accordingly to the catalytically active surface area (H_2 chemisorption) to correspond to 3.3 g/L of pure Pt-CNF (conditions: 0.33 M KOH, 0.06 M glucose, RT).

Data Availability Statement

The data that support the findings of this study are available from the corresponding author upon reasonable request.

Keywords: Glucose dehydrogenation · carbon nanofiber · polyethersulfone · mixed matrix membrane · catalytic membrane

[1] J. Lee, B. Saha, D. G. Vlachos, *Green Chem.* **2016**, *18*(13), 3815–3822.
[2] J. Koch, E. Scott, J. Bitter, A. A. Tashvigh, *Bioresour. Technol.* **2022**, *363*, 127994.
[3] M. P. van der Ham, E. van Keulen, M. T. Koper, A. A. Tashvigh, J. H. Bitter, *Angew. Chem. Int. Ed.* **2023**, *62*(33), e202306701.
[4] R. D. Armstrong, J. Hirayama, D. W. Knight, G. J. Hutchings, *ACS Catal.* **2018**, *9*(1), 325–335.
[5] W.-J. Liu, Z. Xu, D. Zhao, X.-Q. Pan, H.-C. Li, X. Hu, Z.-Y. Fan, W.-K. Wang, G.-H. Zhao, S. Jin, *Nat. Commun.* **2020**, *11*(1), 265.
[6] H. Zhang, J. Zhang, J. Bao, *Bioresour. Technol.* **2016**, *203*, 211–219.
[7] J. Liu, C. Li, H. Niu, D. Wang, C. Xin, C. Liang, *Chemistry* **2022**, *17*(12), e202200138.
[8] J. Dirkx, H. Van der Baan, *J. Catal.* **1981**, *67*(1), 1–13.
[9] H. H. Kasai, A. A. B. Padama, B. Chantaramolee, R. L. Arevalo, Behavior of Hydrogen and Hydrogen-Containing Molecules on Metal Surfaces. vol 71. pp 31–72 Hydrogen and Hydrogen -Containing Molecules on Metal Surfaces. Springer Series in Surface Sciences, 2020
[10] W. Wang, G. Olguin, D. Hotza, M. A. Seelro, W. Fu, Y. Gao, G. Ji, *Renewable Sustainable Energy Rev.* **2022**, *160*, 112124.
[11] X. Zhang, L. J. Durndell, M. A. Isaacs, C. M. Parlett, A. F. Lee, K. Wilson, *ACS Catal.* **2016**, *6*(11), 7409–7417.
[12] Y. Ma, B. Li, X. Zhang, C. Wang, W. Chen, *Front. bioeng. biotechnol.* **2022**, *10*, 864787.
[13] A. P. G. Kieboom, H. van Bekkum, *Recl. Trav. Chim. Pays-Bas* **1984**, *103*(1), 1–12. 10.1002/recl.19841030101.
[14] S. Mozia, *Sep. Purif. Technol.* **2010**, *73*(2), 71–91.
[15] G. Zhang, Y. Yu, Y. Tu, Y. Liu, J. Huang, X. Yin, Y. Feng, *Sep. Purif. Technol.* **2023**, *305*, 122515.
[16] N. Zhang, Y. Wu, G. Yuen, C.-F. de Lannoy, *Sep. Purif. Technol.* **2023**, *312*, 123318.
[17] S. Wang, X. Chen, B. Li, X. Shi, Y. Shi, J. Wang, J. Pan, D. Wan, *Sep. Purif. Technol.* **2022**, *286*, 120493.
[18] H. Lin, Y. Ding, *Polymeric membranes: Chemistry, physics, and applications*, Wiley Online Library, **2020**, pp. 2433–2434.
[19] H. G. Lemos, R. A. Ragio, A. C. S. Conceicao, E. C. Venancio, J. C. Mierzwa, E. L. Subtil, *Chem. Eng. J.* **2021**, *425*, 131772.
[20] A. Asadi Tashvigh, Y. Feng, M. Weber, C. Maletzko, T.-S. Chung, *Ind. Eng. Chem. Res.* **2019**, *58*(25), 10678–10691.
[21] Y. Jiang, J. Sun, X. Yang, J. Shen, Y. Fu, Y. Fan, J. Xu, L. Wang, *Inorg. Chem.* **2021**, *60*(3), 2087–2096.
[22] T. Westermann, T. Melin, *Chem. Eng. Process.* **2009**, *48*(1), 17–28.
[23] M. A. Van Spronsen, J. W. Frenken, I. M. Groot, *Nat. Commun.* **2017**, *8*(1), 429.
[24] M. Führer, T. van Haasterecht, N. Masoud, D. H. Barrett, T. Verhoeven, E. Hensen, M. Tromp, C. B. Rodella, H. Bitter, *ChemCatChem* **2022**, *14*(19), e202200493.
[25] A. A. Tashvigh, L. Luo, T.-S. Chung, M. Weber, C. Maletzko, *J. Membr. Sci.* **2018**, *545*, 221–228.
[26] N. Kong, C. Chen, Q. Zeng, B. Li, L. Shen, H. Lin, *Sep. Purif. Technol.* **2022**, *302*, 122178.
[27] S. Zhang, H. Yin, J. Wang, S. Zhu, Y. Xiong, *Energy* **2021**, *216*, 119285.
[28] R. Rizo, D. Sebastián, J. L. Rodríguez, M. J. Lázaro, E. Pastor, *J. Catal.* **2017**, *348*, 22–28.
[29] A. L. Jongerius, R. W. Gosselink, J. Dijkstra, J. H. Bitter, P. C. Bruijnincx, B. M. Weckhuysen, *ChemCatChem* **2013**, *5*(10), 2964–2972.
[30] C. Schneider, W. Rasband, K. Eliceiri, *Nat Methods* **2012**, *9*, 671–675..
[31] A. Abbadi, H. Van Bekkum, *J. Mol. Catal. A* **1995**, *97*(2), 111–118.
[32] C. Kooyman, K. Vellenga, H. De Wilt, *Carbohydr. Res.* **1977**, *54*(1), 33–44.
[33] I. V. Delidovich, O. P. Taran, L. G. Matvienko, A. N. Simonov, I. L. Simakova, A. N. Bobrovskaya, V. N. Parmon, *Catal. Lett.* **2010**, *140*, 14–21.
[34] X. Zhang, H. Shi, Q. Chi, X. Liu, L. Chen, *Polym. Bull.* **2020**, *77*, 1003–1014.
[35] S. Fonseca, J. C. Paiva, J. Gonçalves, *J. Chem. Educ.* **2008**, *85*(8), 1133.

Manuscript received: December 4, 2023
Revised manuscript received: May 21, 2024
Accepted manuscript online: May 21, 2024
Version of record online: ■■, ■■

RESEARCH ARTICLE

This work provides a proof of concept of a two-membrane system for the catalytic dehydrogenation of glucose to gluconic acid. One is a catalytic active mixed matrix membrane (incorporation of Pt-CNF) that has a high selectivity towards gluconic acid (93%). The other is a H_2 separating membrane with the goal of removing H_2 from the reaction mixture, thereby disrupting the equilibrium and driving the reaction forward.

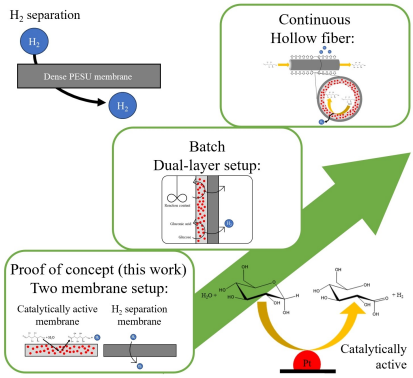

D. van der Made, E. van Keulen, T. van Haasterecht, J. H. Bitter, M. Weber, A. A. Tashvigh**

1 – 13

Mixed Matrix Pt-Carbon Nanofiber Polyethersulfone Catalytic Membranes for Glucose Dehydrogenation